Joined-wing test bed UAV

Dimo Zafirov & Hristian Panayotov

CEAS Aeronautical Journal
An Official Journal of the Council of European Aerospace Societies

ISSN 1869-5582
Volume 6
Number 1

CEAS Aeronaut J (2015) 6:137-147
DOI 10.1007/s13272-014-0134-z

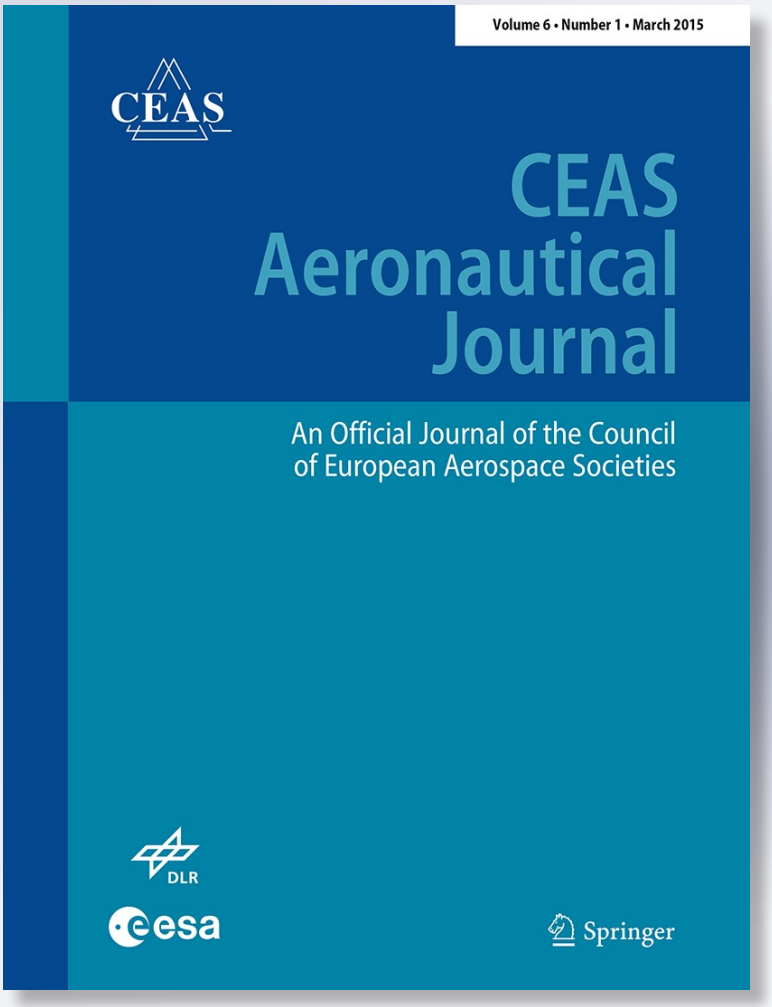

Springer

Your article is protected by copyright and all rights are held exclusively by Deutsches Zentrum für Luft- und Raumfahrt e.V.. This e-offprint is for personal use only and shall not be self-archived in electronic repositories. If you wish to self-archive your article, please use the accepted manuscript version for posting on your own website. You may further deposit the accepted manuscript version in any repository, provided it is only made publicly available 12 months after official publication or later and provided acknowledgement is given to the original source of publication and a link is inserted to the published article on Springer's website. The link must be accompanied by the following text: "The final publication is available at link.springer.com”.

Author's personal copy

CEAS Aeronaut J (2015) 6:137–147
DOI 10.1007/s13272-014-0134-z

ORIGINAL PAPER

Joined-wing test bed UAV

Dimo Zafirov · Hristian Panayotov

Received: 10 December 2013 / Revised: 15 September 2014 / Accepted: 15 September 2014 / Published online: 7 October 2014
© Deutsches Zentrum für Luft- und Raumfahrt e.V. 2014

Abstract The future green aircraft will be required to meet demanding constraints, including weight reduction, high energy and aerodynamic efficiencies and high performance, to be compliant with pollutant emissions and noise generation regulations. The joined-wing concept is considered a trade-off variant for a green aircraft design with a lower cruise drag and lower structural weight. In addition, the requirements for low pollution and noise could be met using an all-electric aircraft. Hence, the aim of the present study is to design and produce a joined-wing unmanned aircraft test bed or flight laboratory. The basic design incorporates tip-joined front and rear wings with wing-tip vertical joints. The airframe is mainly composed of carbon and glass fibre composite materials. The power plant consists of an electric ducted fan, speed controller and Li-Po batteries. The aircraft integrates the Piccolo II Flight Management System, which offers a state-of-the-art navigation and flight data acquisition. Prior to production and flight testing of the prototype, aircraft aerodynamics and flight dynamics were analysed. Potential models with wind tunnel tests have been used to determine aircraft aerodynamics. One of the major problems found during simulation and flight experiments is the Dutch roll effect. This is thoroughly discussed in the paper. Some problems that concern autopilot tuning are also described.

Keywords Joined wing · UAV · Design · Test bed · Studies

1 Introduction

The joined wing is a relatively new concept that, in general, represents a wing configuration that joins the "front" and "rear" wings in a spanwise direction to form a diamond-shaped box. Starting in the 1970s, a great deal of work [1, 2] has been published on joined-wing concepts, aerodynamics, structures and multi-disciplinary optimisation (MDO). However, recently most aircraft design organizations have recalled this concept due to its serious advantages compared to cantilevered wings. These advantages include a lower aerodynamic drag, increased structural strength and/or lower structural weight, direct lift and side-force control. Thus, the joined-wing concept is a contemporary trade-off variant for green transport aircraft or unmanned aerial vehicles (UAVs). To design, produce and operate joined-wing aircraft, much research must be completed, both theoretical and experimental. Hence, the above-mentioned implies the necessity of the development of a joined-wing test bed aircraft or a flying laboratory that could yield real-time flight data for analysis and characteristics determination.

To fulfil this task, a team was formed in the Department of Transportation and Aviation Engineering at the Technical University-Sofia, Plovdiv Branch. The main objectives and expected results reside in the areas of aerodynamics, aircraft structure and flight dynamics. In the present paper, related investigations are reviewed and published.

This paper is based on a presentation at the CEAS Air and Space Conference 2013, September 16–19, Linköping, Sweden.

D. Zafirov · H. Panayotov (✉)
Department of Transportation and Aviation Engineering, Technical University-Sofia, Plovdiv Branch, 4000, 25 Tsanko Dyustabanov Str., Plovdiv, Bulgaria
e-mail: hristian@tu-plovdiv.bg

D. Zafirov
e-mail: zafirov@tu-plovdiv.bg

Author's personal copy

2 JoWi-2 test bed

Figure 1 shows a joined-wing UAV: the JoWi-2FL (FL = Flight Laboratory).

The basic design incorporates tip-joined front and rear wings with wing-tip vertical joints. The front and rear wing root chords are structurally connected using a keel-like element that starts at the fuselage through the propulsion mounting structure and ends at the vertical stabilizer. The role of the keel is to increase the strength and stiffness of the wing. The airframe is mainly composed of carbon and glass fibre composite materials.

Because the main concept aims to describe an all-electric aircraft, the power plant of the UAV is represented by a modern carbon fibre electric ducted fan (EDF) (Fig. 2), powered by Li-Po batteries.

The main advantages of an EDF are its small dimensions, compared to typical propellers at comparable and acceptable efficiency. In the case of a joined-wing design, it is possible to locate the EDF close to or at the aircraft centre of gravity. As a result, in our future work, an option to rotate the EDF to produce a thrust-vectored aircraft will be possible. A transition to a jet-powered aircraft is also an option without changing the basic design.

The joined wing is appropriate for locating and using a great number of control surfaces with different assignments. For example, the JoWi-2FL has nine control surfaces, two at each quarter of the wing and a rudder. It is known that when the control surfaces are used as elevators and ailerons, they are referred to as elevons [elevon = elev(ator) + (ailer)on]. When they are used as flaps and ailerons, they are referred to as flaperons [flaperon = flap + (ail)eron]. With the joined-wing scheme, the rear edge flaps and ailerons can be used as elevators and slope rudders and for direct control of the lift and side force. This could result in the introduction of a new term for joined-wing aircraft, such as flapeleron [flapeleron = flap + ele(vator) + (aile)ron] [2, 3].

The flight controls of the JoWi-2FL include the following: a front wing inboard section, which contains flaps and an elevator (fl.); a front wing outboard section, which contains ailerons (ail); a rear wing inboard section, which contains elevators (elev.); a rear wing outboard section, which contains an elevator and/or ailerons (elevon); and a rudder on the vertical stabilizer (rudd.).

The number of flight controls, in addition to the complex aerodynamics of the joined-wing design, defines such a UAV as a complex aircraft to control. Thus, the problem of integrating a robust autopilot system is significant. Several autopilot systems were considered; however, the Cloud Cap Piccolo II system was finally chosen.

The core of the flight control system (FCS) of the JoWi-2FL aircraft is the Autopilot Piccolo II system (Fig. 3), which offers state-of-the-art navigation and flight data acquisition. Some advanced features of the Piccolo II are as follows:

- Onboard inertial, air data, and GPS sensors, a datalink radio, and an EMI-shielded enclosure;
- Supports operation of a wide variety of UAVs in both fixed wing and VTOL configurations;

Fig. 1 JoWi-2 FL

Fig. 2 Schübeler DS77 DIA HST

Fig. 3 Cloud Cap Piccolo II Autopilot

Author's personal copy

Table 1 JoWi-2FL design parameters

Parameter	Value	Dimension
Wing gross area	0.55	m^2
Wing span	1.8	m
Rear-to-front wing area ratio	1	–
Take-off mass	7.5	kg
Ducted fan thrust	98	N

– Both software and hardware in the loop (SiL/HiL) simulation modes for pre-flight testing, which are critical for a non-conventional aircraft.

The main design parameters of the JoWi-2FL aircraft are given in Table 1.

3 Aerodynamics

To investigate and determine the aerodynamics of the discussed aircraft, potential vortex lattice methods and wind tunnel experiments were used.

4 Potential methods

Athena Vortex Lattice (AVL), developed by Mark Drela of MIT, is used as a potential low-speed wing aerodynamics method and software.

The vortex lattice method (VLM) is a numerical, computational aerodynamics method that is commonly used. Like the panel methods, VLM is based on potential flow theory and the solution of Laplace's equation $\nabla^2\phi = 0$.

This equation is exact when the flow is incompressible, inviscid and irrotational. The incompressible potential flow model provides reliable predictions over a wide range of conditions. For the potential flow assumptions to be valid for aerodynamic calculations, viscous effects must be small, and the flowfield must be subsonic at all locations. Subsonic compressible flow can be modelled if the Prandtl-Glauert transformation is applied.

The key feature of Laplace's equation is the property that allows the equation governing the flowfield to be converted from a 3D problem throughout the field to a 2D problem for finding the potential on the surface. The solution is then found by distributing "singularities" of unknown strength over discretized parts of the surface. The strengths of the singularities are determined by solving a linear set of algebraic equations.

Despite the number of assumptions, the VLM provides remarkable insight into wing aerodynamics and component interaction. The VLM cannot compute the viscous drag, but the induced drag can be reliably estimated.

The VLM is shown in Fig. 4. The lifting and control surfaces are modelled; the fuselage is not considered, as it could yield a methodological error in the results for the lifting system.

The calculated results of the desired aerodynamic characteristics in terms of the angle of attack (AOA) are given in Table 2. These values are necessary for flight dynamics simulations and autopilot tuning.

The following nomenclature is used in Table 2 and throughout the document:

- c is the coefficient of aerodynamic force or moment;
- α and β are the angle of attack and sideslip angle, respectively;

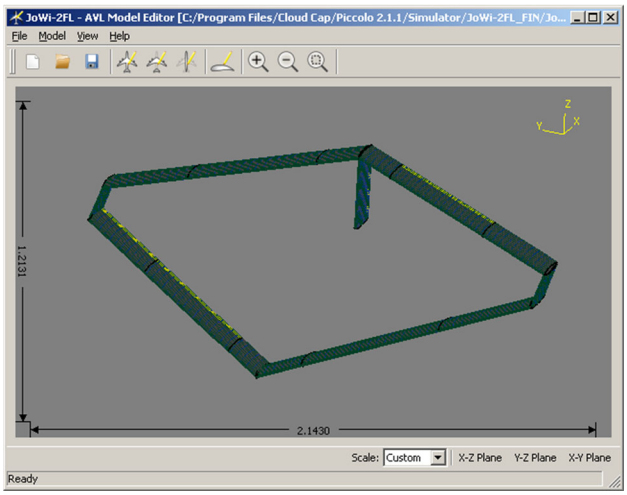

Fig. 4 JoWi-2FL AVL model

Table 2 Aerodynamics properties vs AOA

	$\alpha = -2°$	$\alpha = 2°$	$\alpha = 6°$	$\alpha = 10°$
C_D	0.015	0.021	0.033	0.052
C_L	0.046	0.342	0.634	0.920
$C_{L\alpha}$	4.254	4.223	4.149	4.035
$C_{m\alpha}$	−0.368	−0.402	−0.425	−0.442
$C_{Y\beta}$	−0.579	−0.545	−0.508	−0.468
C_{lp}	−0.497	−0.495	−0.489	−0.479
C_{mq}	−1.345	−1.383	−1.413	−1.437
$C_{L\delta_{fl}}$	0.522	0.506	0.486	0.462
$C_{m\delta_{fl}}$	0.164	0.163	0.160	0.156
$C_{l\delta_{ail}}$	−0.048	−0.046	−0.044	−0.041
$C_{L\delta_{elev}}$	0.702	0.695	0.681	0.660
$C_{m\delta_{elev}}$	−0.351	−0.353	−0.350	−0.345
$C_{l\delta_{elevon}}$	−0.068	−0.067	−0.066	−0.064
$C_{L\delta_{elevon}}$	0.410	0.406	0.396	0.382
$C_{m\delta_{elevon}}$	−0.153	−0.153	−0.152	−0.149
$C_{Y\delta_{rudd}}$	0.131	0.129	0.126	0.121
$C_{n\delta_{rudd}}$	−0.044	−0.043	−0.042	−0.040

Author's personal copy

- L is the aerodynamic lift force;
- D is the aerodynamic drag force;
- X, Y, and Z are the projections of the aerodynamic force on the axes of the body coordinate system;
- L, M, and N are the projections of the aerodynamic moment on the axes of the body coordinate system;
- $\overline{p}, \overline{q}, \overline{r}$ are the dimensionless angular rates, where $\overline{p} = pb/2V$, $\overline{q} = q\overline{c}/2V$, and $\overline{r} = rb/2V$ where $\overline{c}$ is the mean aerodynamic chord and b is wingspan;
- δ is the angle of the control surface deflection.

For example, $C_{L\alpha}$ is the partial derivative of the lift coefficient with respect to the angle of attack in radians or the lift curve slope. $C_{m\delta_{\text{elev}}}$ is the partial derivative of the pitch moment coefficient with respect to the angle of deflection of the elevator in radians, among others.

5 Wind tunnel tests

Wind tunnel tests are conducted to validate the accuracy of the potential methods. The test wind tunnel and the joined-wing model are shown in Fig. 5a and b.

The wind tunnel is a Russian made ULAK-1 (Russian: Учебно-лабораторный аэродинамический комплекс). It has an open working area with a nozzle cross-section of 600 × 400 mm. The maximum allowed model span is 400 mm, and the maximum model cross-sectional area is 1,800 mm^2. The wind speed can be varied from 2 to 60 m/s. The experiment is fully automated.

The experimental results are given in Figs. 6, 7, and 8. The effective Reynolds number is Re = 129,886, as calculated using the wind tunnel airspeed, joined-wing standard mean chord length and wind tunnel turbulence factor.

An interesting result is that the "classical" peak value of the lift coefficient that is expected as the AOA is increased is not observed (Fig. 6). There is rather some decrease of the lift curve slope as the AOA is increased, but the maximum lift coefficient $C_{L,\max}$ is not reached at the maximum limit angle of attack for this wind tunnel. A similar phenomenon can be observed for the pitch moment coefficient: the typical inflection point is missing.

The conclusion can be made that the joined wing will be able to maintain relatively high AOA at low stall speeds and will have a "nose down" stall tendency.

6 Ducted fan aerodynamics

As described above, an electric ducted fan (Fig. 2) is used as the propulsion unit on the JoWi-2FL. For the purpose of flight dynamics simulations and flight experiments, the thrust of the power plant is required.

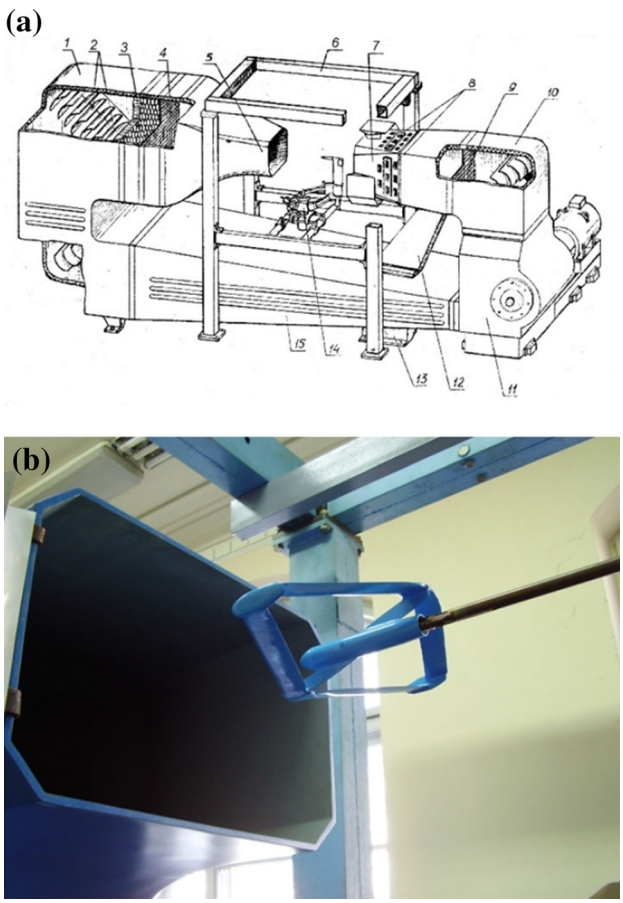

Fig. 5 Wind tunnel (**a**) and joined-wing model (**b**)

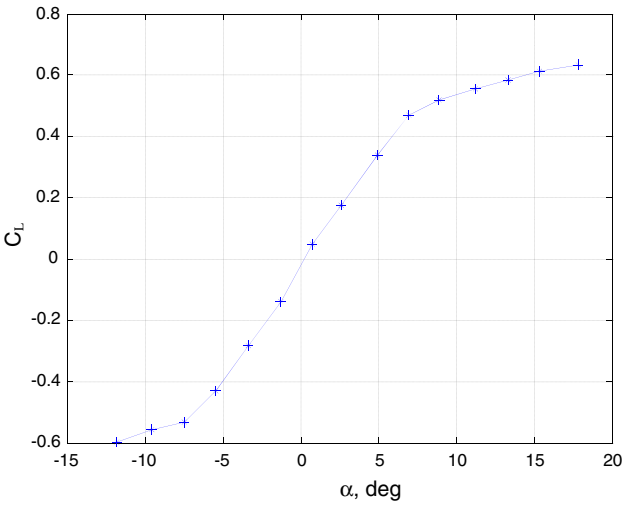

Fig. 6 Lift coefficient vs. AOA (experimental)

6.1 1-ducted fan; 2-linear bearing; 3-load cell

Because the geometry of the fan blades is not known, a theoretical calculation of the fan's thrust is not possible. In this

Author's personal copy

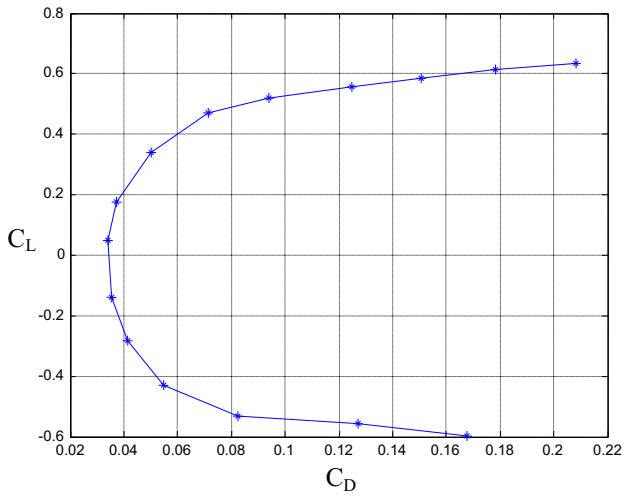

Fig. 7 Drag polar (experimental)

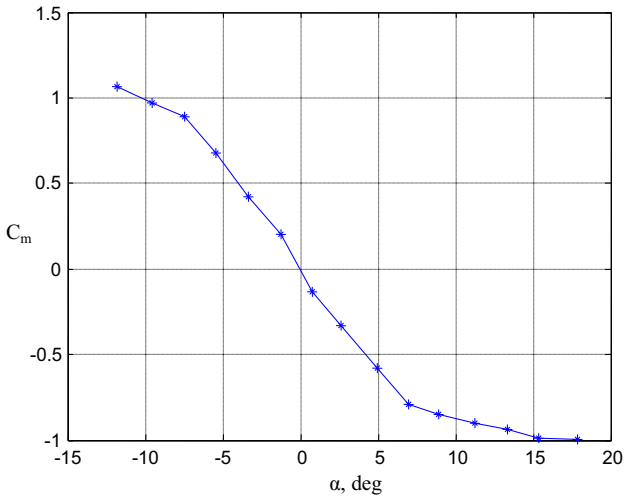

Fig. 8 Pitch moment coefficient (experimental)

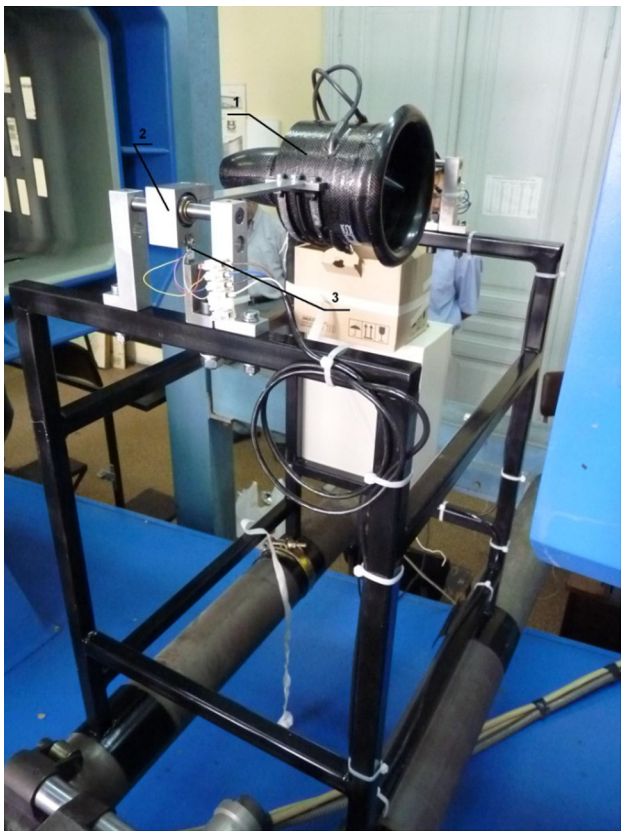

Fig. 9 Ducted fan thrust measurement equipment. *1* ducted fan, *2* linear bearing, *3* load cell

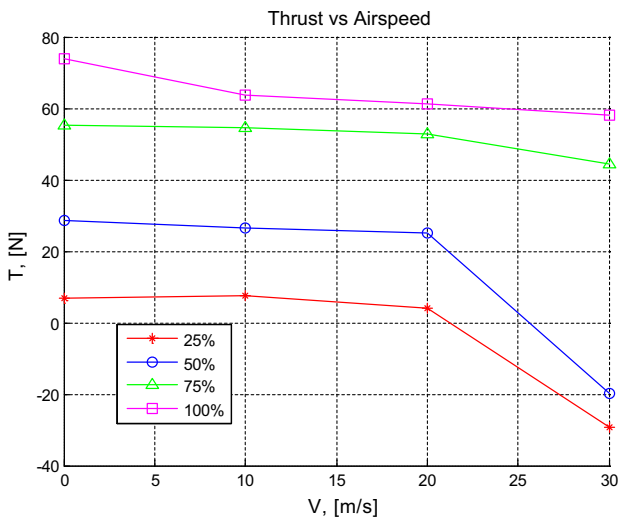

Fig. 10 Thrust vs. airspeed

study, the dependence of the thrust and fan efficiency is determined experimentally in the wind tunnel. Specially designed thrust measurement equipment is used so that the propulsion unit is placed in the working area of the wind tunnel (Fig. 9). The results for the ducted fan thrust are shown in Fig. 10. The power of the electrical motor is given in percent. Figure 11 gives the efficiency as a function of airspeed. The efficiency is calculated using the following formula:

$$\eta_{\mathrm{EDF}} = TV/P, \tag{1}$$

where T is the thrust in N; V is the airspeed in m/s; P is the electrical power of the engine in W.

The "negative" thrust measured at low power (25 % and 50 %), as shown in Fig. 10, indicates that the AOA of the fan blades becomes smaller than the zero-lift AOA. As the power is increased, the circumferential speed (i.e. rpm) is also increased, and the AOA becomes positive or larger than the zero-lift AOA. This is why the zero-thrust regime at higher powers occurs at much higher airspeeds. The maximum measured efficiency for the ducted fan and the motor together is approximately 0.65 at an airspeed of 70 m/s.

Author's personal copy

7 Simulations

Simulations are conducted to estimate the aircraft's flight dynamics and analyse flight performance. This is done at an early design stage, such as conceptual design, to eliminate undesired flight behaviour. As will be described later, the simulations show that, at low airspeeds and high AOA, Dutch roll mode occurs.

The simulations are run using the MATLAB Simulink Aerospace Blockset and the Piccolo II Simulation Environment. The first one gives more freedom to analyse aircraft flight using various configurations of the control surfaces, while the second allows for flying the aircraft in an integrated aircraft-autopilot simulation environment.

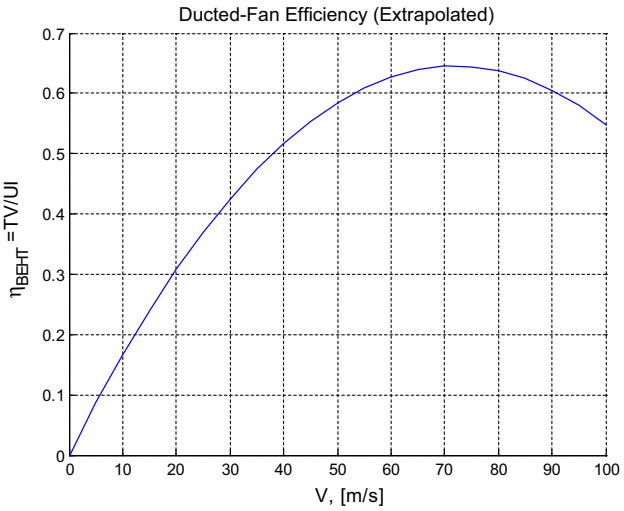

Fig. 11 Ducted fan efficiency

8 Simulation models

The simulation model of the aircraft's flight dynamics is shown in Fig. 12. It generally consists of the following submodels that are designed in the MATLAB Simulink Aerospace Blockset:

1. Longitudinal movement
2. Side-lateral movement
3. Propulsion
4. Six degree-of-freedom flight dynamics
5. Standard atmosphere
6. Earth gravity
7. Flight controls
   Flight gear interface

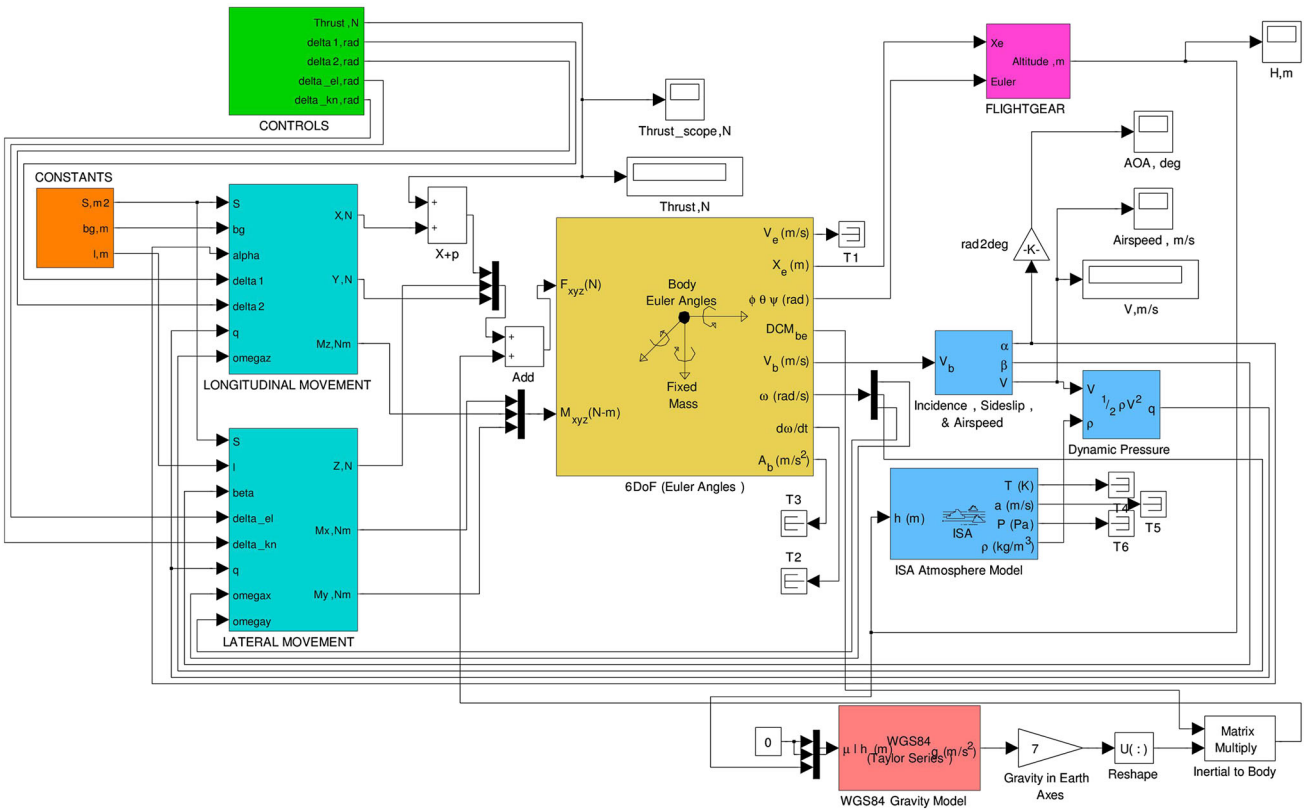

Fig. 12 Simulation model

Author's personal copy

Because we have previously determined the aerodynamic coefficients and their derivatives, the ducted fan characteristics and the desired flight modes, a flight simulation of the JoWi-2FL is possible.

An interface with the flight gear flight simulator is established, and the flight is visualized during the simulation (Fig. 13). A joystick is used as an input for the flight controls.

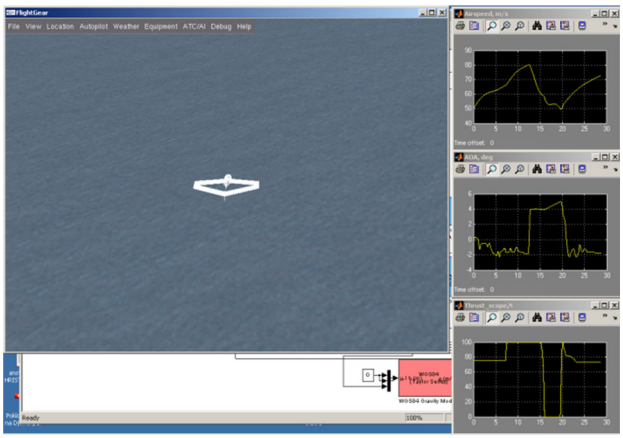

Fig. 13 Visualization with flight gear

9 HiL and SiL simulations

The Piccolo II autopilot system offers its own simulation environment tools that include hardware-in-the-loop (HiL) and software-in-the-loop (SiL) simulations (Fig. 14).

The HiL simulation uses the Piccolo II autopilot system and Ground Control Station (GCS) hardware during the flight simulation, allowing the simulated aircraft to respond as if it were actually flying. The SiL simulation uses software models for the autopilot and GCS. Simulation allows the flight control laws for the aircraft and mission functionality to be tested without risking a real aircraft in a test flight.

10 Piccolo II autopilot tuning

Autopilot tuning requires certain vehicle data to be input [4]. These include geometrical properties, mass and inertial properties, propulsion characteristics and aerodynamic characteristics, which are the most critical. The Piccolo CGS software, called the Piccolo Command Centre, is designed to automatically calculate these values from AVL data, but in the case of the joined-wing configuration with nine control surfaces, errors occur and the output XML file is empty. Therefore, these values are manually calculated. They are as follows:

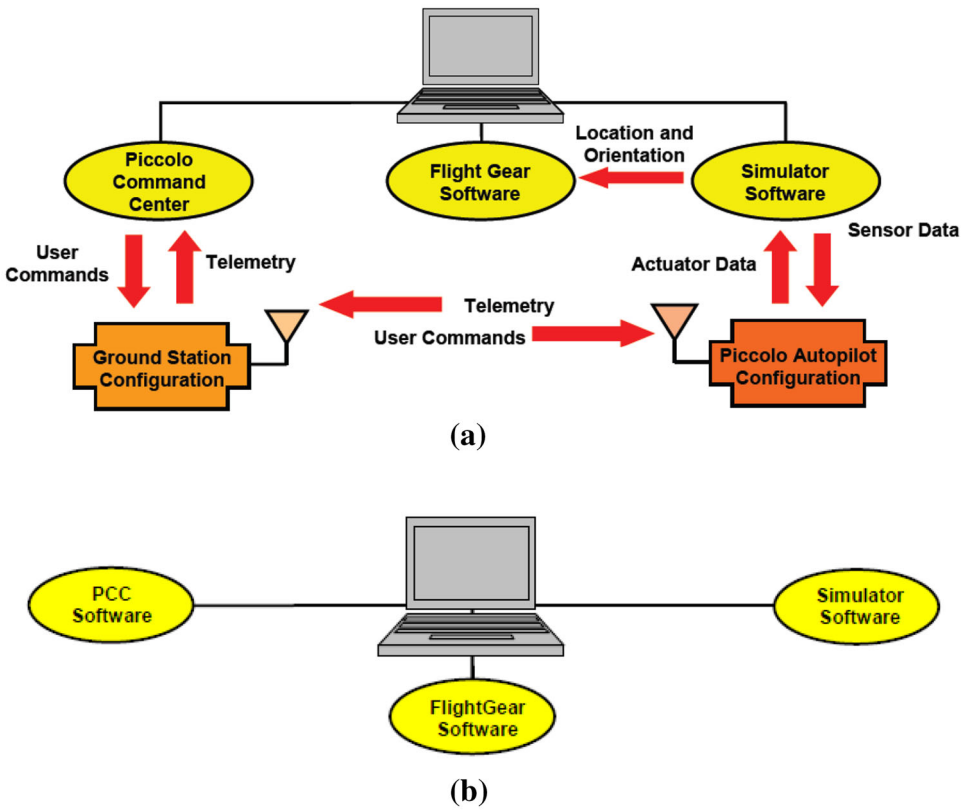

Fig. 14 HiL (**a**) and SiL (**b**) configurations

Author's personal copy

1. Elevator power—change in pitch moment coefficient per change in elevator, 1/rad. Increasing elevator angles should produce decreasing pitch moments. Hence this number is negative. If only elevators are used for pitch control it is equal to $C_{m\delta_{\text{elev}}}$ from Table 2. If elevons are used with elevators then the superposition rule should be applied.

2. Elevator effectiveness—steady-state change in lift coefficient per change in elevator position, 1/rad. This is the primary elevator control power term. The change in the lift is both due to change in the lift from the elevator and from the respectful change in the angle of attack. This value is calculated using the formula:

$$\sum c_{L\delta_{\text{elev}}} = c_{L\delta_{\text{elev}}} + c_{L\alpha}\frac{c_{m\delta_{\text{elev}}}}{c_{m\alpha}}. \tag{2}$$

3. Aileron effectiveness—dimensionless roll rate per change in aileron position, 1/rad. This is the primary aileron control power term.

$$\bar{p}_{\delta_{\text{ail.}}} = \frac{\partial \bar{p}}{\partial \delta_{\text{ail.}}} = \frac{\partial c_l/\partial \delta_{\text{ail}}}{\partial c_l/\partial \bar{p}} = \frac{c_{l\delta_{\text{ail.}}}}{c_{lp}}. \tag{3}$$

where $\bar{p}$ is the dimensionless roll rate.

4. Rudder power—yawing moment coefficient per change in rudder position, 1/rad. This is the primary rudder control power term. It equals $C_{n\delta_{rudd}}$ from Table 2.
5. Rudder effectiveness—change in sideslip per change in rudder position. In combination with the tail moment arm this number is used to estimate the amount of rudder deflection required to coordinate a turn.

$$\beta_{\delta_{\text{rudd}}} = \frac{\partial \beta}{\partial \delta_{\text{rudd}}} = \frac{\partial c_Y/\partial \delta_{\text{rudd}}}{\partial c_Y/\partial \beta} = \frac{c_{Y\delta_{\text{rudd}}}}{c_{Y\beta}} \tag{4}$$

6. Sideslip effect—change in side-force coefficient per change in side slip, 1/rad. This term is used to scale the side-force integral feedback for feedback turn coordination. It equals $C_{Y\beta}$ from Table 2.

The values for the discussed autopilot tuning coefficients are given in Table 3.

Table 3 Autopilot tuning coefficients

Elevator power	Elevator effectiveness	Aileron effectiveness
−0.36	−4.37	0.09
Rudder power	Rudder effectiveness	Sideslip effect
0.09	−0.35	−0.74

The data in Table 3 are used to define the gains in the longitudinal and lateral control feedbacks of the universal PID controller that the autopilot uses.

For example, we can examine the elevator effectiveness coefficient. Under steady-state assumptions if the aircraft is statically stable. The angle of attack and hence the lift coefficient are assumed to depend linearly on the elevator according to this term and the "C_L at zero elevator". The controller uses this number to predict the correct elevator position based upon the acceleration command and to scale the elevator feedback gains. Reducing this value causes the controller to move the elevator further.

The aileron effectiveness is a similar property in the lateral control. Under steady-state assumptions if the roll damping is large and the roll axis inertia is small, the dimensionless roll rate depends only on the aileron angle according to this term. The controller uses this number to predict the correct aileron position and scale the aileron feedback gains. Reducing this value causes the controller to move the aileron further.

11 Dutch roll considerations

It might be of use to discuss that during simulations the initial JoWi-2FL design showed strong Dutch roll effect at low speeds. This made the landing difficult and risky. The Dutch roll effect is mainly due to increased lateral stability coefficient ($C_{l\beta}$) compared to directional stability coefficient (weathercock stability) ($C_{n\beta}$). The joined-wing design having backswept forward wing and foreswept rear wing both of which obtaining specific dihedral/anhedral angle could seriously suffer Dutch roll. One might erroneously consider that the front and rear wings have approximately the same dihedral/anhedral angles and, thus, that the roll stability of both wings should be acceptable. However, the patterns of the flow over the front and rear wings differ due to the wings' backswept angle. Previous investigations [5, 6] at the same AOA show that the lift coefficient of the front wing is generally significantly higher than that of the rear wing. As a result, the roll stability effect of the front wing is expected to be higher than the roll stability effect of the rear wing. Finally, a joined wing with a typical diamond shape, as viewed from the front, has high potential for Dutch roll, primarily at low speeds and high AOA. The initial design of the JoWi-2FL indeed showed strong Dutch roll during landing. Because the only practical way to minimize this effect was to increase the vertical stabilizer area, design variants with increased vertical stabilizer area were considered. This problem was not resolved until the vertical stabilizer area was increased significantly [7]. To determine the new stabilizer area, calculations and simulations

Author's personal copy

Table 4 Lateral and directional stability

$\alpha.^\circ$	$C_{l\beta}$		$C_{n\beta}$		κ	
	Basic	New	Basic	New	Basic	New
−2	−0.088	−0.118	0.056	0.117	1.918	1.221
0	−0.099	−0.127	0.052	0.115	2.331	1.343
2	−0.111	−0.136	0.049	0.112	2.769	1.465
4	−0.123	−0.145	0.047	0.111	3.210	1.584
6	−0.135	−0.154	0.045	0.110	3.629	1.698
8	−0.148	−0.163	0.045	0.110	3.998	1.802
10	−0.160	−0.172	0.045	0.110	4.292	1.896

were performed. The Dutch roll effect is likely to occur when the parameter $\kappa > 2$:

$$\kappa \approx -\frac{C_{l\beta}}{C_{n\beta}} \times \frac{J_z}{J_x}. \tag{5}$$

where $J_x \times J_z$ are the mass inertia moments for the specified axes of body reference system.

Table 4 shows this parameter, calculated for the basic design and for the increased stabilizer area variant. A quick analysis of Table 4 shows that for the basic variant at an AOA of more than 4°, the parameter κ exceeds the norm ($\kappa > 2$) and, thus, that Dutch roll is expected to occur. This is because of the small weathercock stability $C_{n\beta}$ as compared to $C_{l\beta}$. When the vertical stabilizer area is increased (new variant in Table 4), the $C_{n\beta}$ nearly doubles and the parameter κ is smaller ($\kappa < 2$) as is desirable. Mass moments of inertia are theoretically calculated and experimentally measured using the physical pendulum method [8].

This periodic instability is also visible from simulation data [6] in Fig. 15 at an airspeed of 15 m/s using the simulation model given in Fig. 12. The change of yaw and roll angles is given versus time as a reaction to a short disturbance.

It is visible that the amplitude attenuation of both angles is weak for the basic variant. This is improved when the vertical stabilizer area is increased, although weak Dutch roll effects are still observed, but now at lower airspeeds. These results were confirmed in real flights. Usually, at landing, an initially strong Dutch roll mode was observed with high amplitudes, primarily of the roll angle, which is shown also in the simulations.

12 Flight experiments

The first flight of the JoWi-2FL test bed was conducted at Cheshnegirovo airfield near the city of Plovdiv, Bulgaria (Fig. 16).

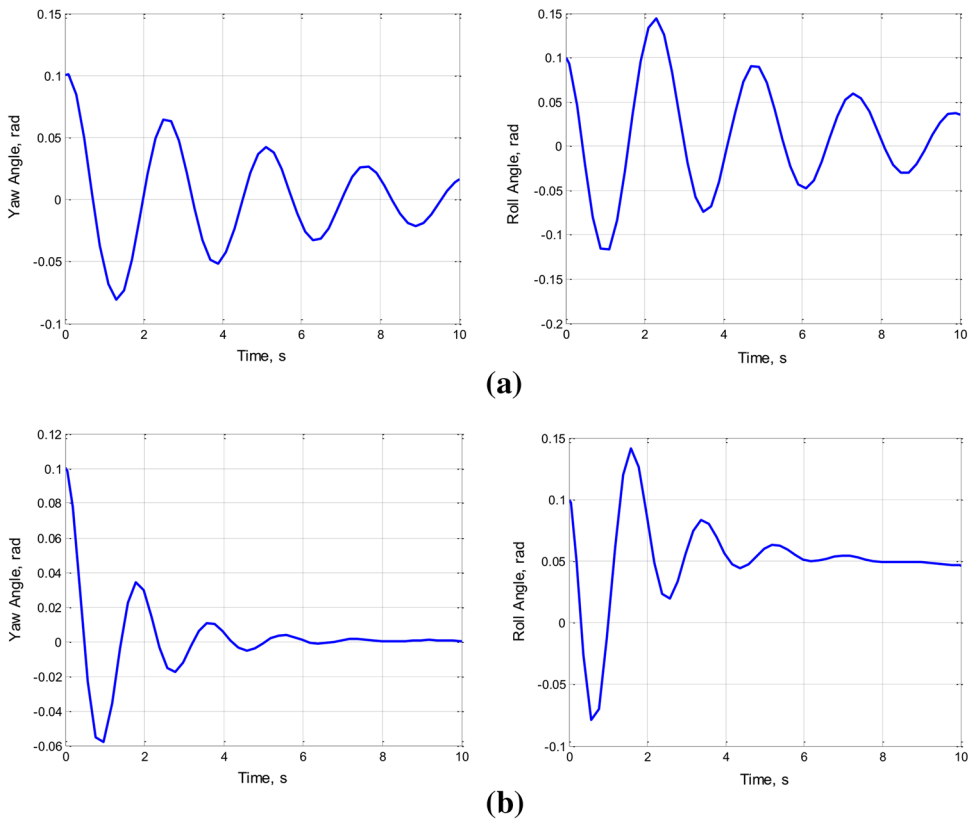

Fig. 15 Yaw (*left*) and roll (*right*) angles. **a** Basic variant, **b** Increased fin area

Author's personal copy

Fig. 16 JoWi-2FL maiden flight

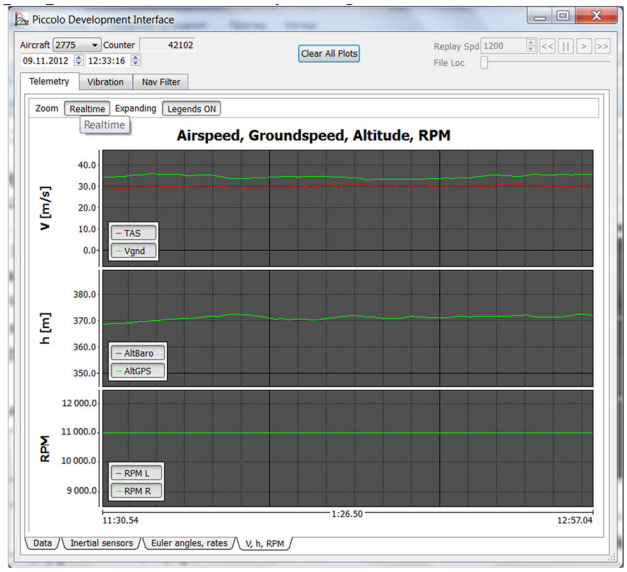

Fig. 18 Autopilot control

The flight mission is shown in Fig. 17. The figure shows the change of altitude and airspeed in time, as measured barometrically and by GPS. The aircraft was flown entirely manually to check aircraft performance, stability and control.

Further flights were conducted using the Piccolo II autopilot system. In the autonomous mode, the aircraft held its mission settings precisely without any human interaction. Figure 18 shows the accuracy of airspeed, altitude and engine RPM stabilization in autopilot mode. As shown, the deviation from the initial assignments of these parameters is acceptable and allows the aircraft to be navigated precisely in autopilot mode. Further analysis is needed to assess quantitatively the accuracy of control and stabilization.

During the preparation of the flight experiments, SiL and HiL simulations were extremely helpful. Thanks to a precisely built simulation model, many issues were uncovered and corrected early on in the design process; the most significant problem that was corrected was the Dutch roll mode, as explained above. HiL simulations were helpful to analyse the deflections of the flight controls. With nine flight controls located on this UAV, programming of the autopilot is difficult. HiL simulations allowed for the accurate measurement and observation of the deflection of the flight controls. Finally, flight missions were simulated before the real first flight was made, also reducing risk.

These steps were critical for the safety and the success of the first flight. In addition, precise calculations of aircraft aerodynamics, propulsion, and mass and inertia properties are necessary for accurate results.

Fig. 17 Manual control

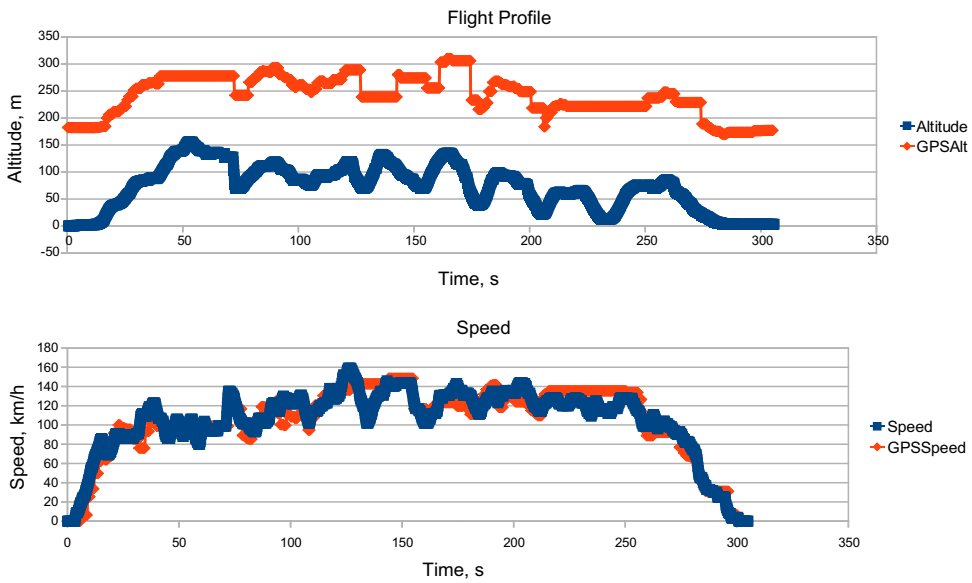

Author's personal copy

13 Conclusion

A joined-wing UAV test bed was designed, produced and flown. Numerous simulations and ground and flight experiments were conducted to precisely determine aircraft performance. The JoWi-2FL aircraft is shown to be capable of fully autonomous operation as an onboard experimental test bed. It will be used for real-time flight data acquisition for aerodynamics and flight performance analysis. It could also be used to solve tasks related to autonomous control and navigation.

References

1. Wolkovitch, J.: The joined wing: an overview. J Aircr **23**, 161–178 (1986)
2. Zafirov, D.: Joined wings thrust vectored UAV flight envelope. In: AIAA-2010-7509, AIAA Atmospheric Flight Mechanics Conference, Toronto, (2010)
3. Zafirov, D.: Joined wing with ducted fan. UAV World Conference on Disc [CD-ROM], Exhibition Centre Frankfurt/Main, Frankfurt am Main (2009)
4. Vaglienti, B., Hoag, R., Niculescu, M.: Piccolo User's Guide v2.1.1. Cloud Cap Technology, Hood River, OR (2010)
5. Zafirov D., Panayotov H.: Experimental results analysis of joined-wing aircrafts. In: Scientific Conference on Aeronautics, Automotive and Railway Engineering and Technologies BulTrans-2012, Sozopol, Bulgaria, 82–85, (2009)
6. Panayotov H., Zafirov D.: Aerodynamic optimization of joined-wing for unmanned aerial vehicle. J. Tech. Univ. Plovdiv, "Fundamental Sciences and Applications" **13**, 12–19 (2006)
7. Panayotov H.: Investigation of Dutch roll of a joined-wing aircraft. In: Scientific Conference on Aeronautics, Automotive and Railway Engineering and Technologies BulTrans-2012, Sozopol, Bulgaria, 26–28, 84–87, (2012)
8. Zafirov D.: Mass moments of inertia of joined-wing unmanned aerial vehicle. Int. J. Res. Eng. Technol. **2**, 2319–1163 (2013)